Gourbet, L., Yang, R., Fellin, M.G., Paquette, J.-L., Willett, S.D., Gong, J.F., and Maden, C., 2019, Evolution of the Yangtze River network, southeastern Tibet: Insights from thermochronology and sedimentology: Lithosphere, https://doi.org/10.1130/L1104.1
GSA Data Repository Item 2019409

Supplementary Material

1. Sampling and field observations

Figure S1

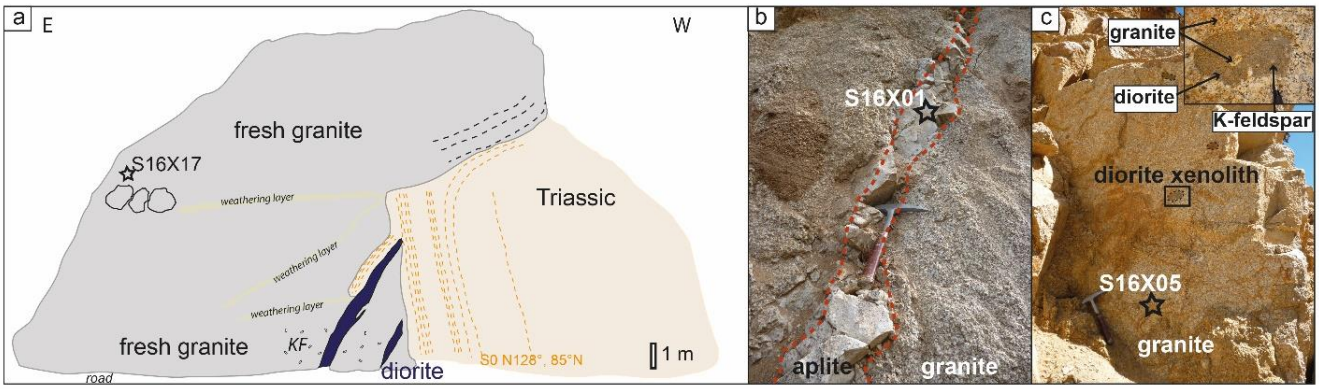

Figure S1. a. Field sketch showing the granite intrusion into Triassic sandstones at site 1. Differential weathering of the granite is related to recent exposure due to the road construction. Star indicates sample location. *KF*: K-feldspar. b. Aplite dyke cutting through the granite (site 2). c. Outcrop at site 2 showing granite with a porphyric texture. Upper right corner: close-up of a diorite xenolith.

Gourbet, L., Yang, R., Fellin, M.G., Paquette, J.-L., Willett, S.D., Gong, J.F., and Maden, C., 2019, Evolution of the Yangtze River network, southeastern Tibet: Insights from thermochronology and sedimentology: Lithosphere, https://doi.org/10.1130/L1104.1
GSA Data Repository Item 2019409

Supplementary Table ST1: Samples location and lithology description

Sample	Latitude (°)	Longitude (°)	Elevation (m)	Lithology
Site 1				
S16X15	28.9900	99.9398	3666	granite
S16X16	28.9919	99.9347	3595	granite
S16X17	28.9952	99.9238	3503	granite
Road				
S16X14	28.9694	99.8393	2829	sandstone
Site 2				
S16X08	28.7984	99.9533	3924	granite
S16X05	28.7980	99.9477	3894	granite
S16X04	28.7921	99.9402	3818	granite
S16X03	28.7952	99.9344	3724	granite
S16X01	28.7968	99.9275	3656	granite
Site 3				
S16X10	28.6910	99.9204	3873	granite
S16X11	28.6952	99.9193	3727	granite
S16X09B	28.7019	99.9155	3621	granite
S16X12	28.7017	99.9117	3452	granite
S16X09	28.7025	99.9076	3378	granite
S16X13	28.7065	99.9058	3321	granite
Site 4				
S16X19	28.530615	99.67482	2790	weathered granite

Gourbet, L., Yang, R., Fellin, M.G., Paquette, J.-L., Willett, S.D., Gong, J.F., and Maden, C., 2019, Evolution of the Yangtze River network, southeastern Tibet: Insights from thermochronology and sedimentology: Lithosphere, https://doi.org/10.1130/L1104.1
GSA Data Repository Item 2019409

2. U-Pb dating of zircon

Supplementary table ST2: Zircon U-Pb data obtained by *in situ* Laser Ablation ICP-MS

S16X01						2 σ error		2 σ error	Rho	Age (Ma)	2 σ error
zircon	Pb ppm[1]	Th ppm[1]	U ppm[1]	Th/U	$^{207}Pb/^{235}U$[2]	$^{207}Pb/^{235}U$	$^{206}Pb/^{238}U$[2]	$^{206}Pb/^{238}U$		$^{206}Pb/^{238}U$	$^{206}Pb/^{238}U$
X01/01	15	431	1140	0.38	0.1004	0.0033	0.01283	0.00036	0.86	82.2	2.4
X01/02	11	403	780	0.52	0.0852	0.0032	0.01292	0.00039	0.79	82.8	2.4
X01/03	9.1	304	675	0.45	0.0859	0.0034	0.01296	0.00039	0.77	83.0	2.4
X01/04	18	251	1439	0.17	0.1025	0.0034	0.01293	0.00039	0.91	82.8	2.4
X01/05	7.1	245	528	0.46	0.0862	0.0035	0.01295	0.00039	0.73	82.9	2.4
X01/06	9.9	482	691	0.70	0.0920	0.0036	0.01286	0.00039	0.77	82.4	2.4
X01/07	8.2	339	598	0.57	0.0867	0.0035	0.01284	0.00039	0.76	82.2	2.4
X01/08	9.9	357	732	0.49	0.0850	0.0040	0.01280	0.00039	0.65	82.0	2.4
X01/09	9.5	241	738	0.33	0.0874	0.0037	0.01289	0.00039	0.71	82.5	2.4
X01/10	35	2946	2083	1.41	0.0862	0.0030	0.01290	0.00036	0.80	82.7	2.4
X01/11	16	669	1153	0.58	0.0891	0.0032	0.01295	0.00039	0.83	82.9	2.4
X01/12	8.1	372	568	0.65	0.0941	0.0039	0.01298	0.00039	0.72	83.2	2.4
X01/13	3.3	159	224	0.71	0.0900	0.0056	0.01317	0.00039	0.47	84.3	2.6
X01/14	16	920	1038	0.89	0.0873	0.0031	0.01309	0.00039	0.84	83.8	2.4
X01/15	12	408	834	0.49	0.0896	0.0034	0.01319	0.00039	0.79	84.5	2.4
X01/16	7.2	411	485	0.85	0.0862	0.0037	0.01282	0.00039	0.71	82.1	2.4
X01/17	11	452	800	0.56	0.0884	0.0034	0.01298	0.00039	0.79	83.2	2.4
X01/18	14	507	1045	0.48	0.0898	0.0032	0.01308	0.00039	0.83	83.8	2.4
X01/19	9.4	393	647	0.61	0.0941	0.0036	0.01309	0.00039	0.78	83.8	2.4
X01/20	15	572	1049	0.55	0.0874	0.0032	0.01305	0.00039	0.82	83.6	2.4
X01/21	42	2527	2795	0.90	0.0867	0.0028	0.01285	0.00036	0.87	82.3	2.3
X01/22	6.1	207	455	0.46	0.0867	0.0038	0.01304	0.00039	0.68	83.5	2.4
X01/23	11	441	753	0.59	0.0880	0.0034	0.01303	0.00039	0.78	83.5	2.4
X01/24	6.4	166	497	0.33	0.0951	0.0039	0.01297	0.00039	0.73	83.1	2.4
X01/25	11	509	800	0.64	0.0875	0.0033	0.01301	0.00039	0.79	83.3	2.4
X01/26	8.8	474	607	0.78	0.0871	0.0034	0.01298	0.00039	0.77	83.1	2.4
X01/27	36	260	2991	0.09	0.0919	0.0031	0.01297	0.00036	0.83	83.1	2.4
X01/28	14	327	1106	0.30	0.0879	0.0032	0.01296	0.00036	0.75	83.0	2.4
X01/29	37	721	2920	0.25	0.0928	0.0031	0.01302	0.00036	0.82	83.4	2.4
X01/30	13	760	857	0.89	0.0867	0.0033	0.01289	0.00036	0.73	82.6	2.4
X01/31	29	959	2193	0.44	0.0881	0.0032	0.01297	0.00036	0.78	83.1	2.4
X01/32	11	579	754	0.77	0.0880	0.0034	0.01294	0.00036	0.73	82.9	2.4
X01/33	14	255	1100	0.23	0.0921	0.0032	0.01303	0.00036	0.79	83.5	2.4
X01/34	4.7	168	289	0.58	0.1021	0.0049	0.01503	0.00045	0.63	96.2	2.8
X01/35	10	392	725	0.54	0.0948	0.0036	0.01286	0.00036	0.74	82.4	2.3
X01/36	10	365	761	0.48	0.0867	0.0033	0.01296	0.00036	0.72	83.0	2.4
X01/37	19	484	1468	0.33	0.0893	0.0031	0.01293	0.00036	0.81	82.8	2.3
X01/38	13	525	927	0.57	0.0866	0.0032	0.01293	0.00036	0.75	82.8	2.3

S16X10						2 σ error		2 σ error	Rho	Age (Ma)	2 σ error
zircon	Pb ppm[1]	Th ppm[1]	U ppm[1]	Th/U	$^{207}Pb/^{235}U$[2]	$^{207}Pb/^{235}U$	$^{206}Pb/^{238}U$[2]	$^{206}Pb/^{238}U$		$^{206}Pb/^{238}U$	$^{206}Pb/^{238}U$
X10/01	4	123	262	0.47	0.0889	0.0046	0.01319	0.00045	0.66	84.5	2.8
X10/02	14	678	916	0.74	0.0886	0.0038	0.01310	0.00042	0.74	83.9	2.8

X10/03	5	155	338	0.46	0.0876	0.0038	0.01286	0.00042	0.75	82.3	2.7
X10/04	4	103	337	0.31	0.0851	0.0039	0.01304	0.00042	0.71	83.5	2.7
X10/05	39	959	2925	0.33	0.0887	0.0032	0.01330	0.00042	0.87	85.2	2.8
X10/06	13	354	977	0.36	0.0870	0.0034	0.01318	0.00042	0.82	84.4	2.7
X10/07	6	184	419	0.44	0.0912	0.0039	0.01305	0.00042	0.75	83.6	2.7
X10/08	27	1601	1751	0.91	0.0903	0.0033	0.01342	0.00042	0.86	85.9	2.8
X10/09	18	566	1292	0.44	0.0881	0.0033	0.01329	0.00042	0.84	85.1	2.7
X10/10	21	623	1532	0.41	0.0883	0.0033	0.01326	0.00042	0.86	84.9	2.7
X10/11	18	560	1376	0.41	0.0866	0.0033	0.01315	0.00042	0.85	84.2	2.7
X10/12	8	315	560	0.56	0.0862	0.0036	0.01297	0.00042	0.77	83.1	2.7
X10/13	10	338	712	0.47	0.0876	0.0035	0.01312	0.00042	0.80	84.0	2.7
X10/14	9	234	721	0.33	0.0876	0.0033	0.01305	0.00042	0.85	83.6	2.7
X10/15	6	298	440	0.68	0.0857	0.0035	0.01287	0.00042	0.80	82.4	2.6
X10/16	5	163	363	0.45	0.0860	0.0048	0.01280	0.00042	0.59	82.0	2.7
X10/17	9	419	646	0.65	0.0862	0.0033	0.01307	0.00042	0.85	83.7	2.7
X10/18	7	219	533	0.41	0.0880	0.0038	0.01307	0.00042	0.74	83.7	2.7
X10/19	14	391	1050	0.37	0.0950	0.0038	0.01321	0.00042	0.79	84.6	2.7
X10/20	19	513	1434	0.36	0.0866	0.0032	0.01305	0.00042	0.88	83.6	2.6
X10/21	8	262	601	0.44	0.0865	0.0039	0.01291	0.00042	0.72	82.7	2.7
X10/22	10	526	665	0.79	0.0873	0.0034	0.01316	0.00042	0.81	84.3	2.7
X10/23	6	224	460	0.49	0.0862	0.0038	0.01295	0.00042	0.74	83.0	2.7
X10/24	2	87	167	0.52	0.0890	0.0051	0.01319	0.00045	0.60	84.5	2.8
X10/25	9	306	695	0.44	0.0881	0.0034	0.01304	0.00042	0.84	83.5	2.6
X10/26	7	432	443	0.98	0.0851	0.0038	0.01293	0.00042	0.73	82.8	2.6
X10/27	9	315	659	0.48	0.0933	0.0035	0.01310	0.00042	0.84	83.9	2.6
X10/28	19	551	1417	0.39	0.0871	0.0031	0.01311	0.00042	0.89	84.0	2.6
X10/29	10	405	692	0.59	0.0859	0.0033	0.01308	0.00042	0.83	83.8	2.6
X10/30	10	431	745	0.58	0.0957	0.0035	0.01305	0.00042	0.87	83.6	2.6
X10/31	8	210	641	0.33	0.0853	0.0035	0.01296	0.00042	0.79	83.0	2.6
X10/32	13	573	924	0.62	0.0873	0.0032	0.01313	0.00042	0.87	84.1	2.6
X10/33	14	417	1074	0.39	0.0884	0.0032	0.01314	0.00042	0.90	84.1	2.6
X10/34	7	375	439	0.85	0.0874	0.0042	0.01314	0.00042	0.66	84.1	2.7
X10/35	3	112	217	0.51	0.0869	0.0065	0.01311	0.00045	0.46	83.9	2.9
X10/36	7	283	526	0.54	0.0853	0.0037	0.01306	0.00042	0.75	83.7	2.6
X10/37	11	437	765	0.57	0.0858	0.0032	0.01308	0.00042	0.86	83.8	2.6
X10/38	2	93	168	0.55	0.0861	0.0061	0.01319	0.00045	0.48	84.5	2.9
X10/39	6	226	466	0.49	0.0867	0.0037	0.01314	0.00042	0.76	84.1	2.6
X10/40	11	392	807	0.49	0.0861	0.0032	0.01296	0.00042	0.87	83.0	2.6
X10/41	7	641	392	1.64	0.0860	0.0040	0.01301	0.00042	0.69	83.3	2.6
X10/42	12	740	790	0.94	0.0868	0.0033	0.01308	0.00042	0.85	83.8	2.6
X10/43	20	857	1450	0.59	0.0853	0.0030	0.01289	0.00039	0.86	82.6	2.6
X10/44	9	470	665	0.71	0.0849	0.0033	0.01292	0.00039	0.78	82.7	2.6
X10/45	5	254	367	0.69	0.0892	0.0040	0.01302	0.00042	0.73	83.4	2.6
X10/46	14	566	1046	0.54	0.0867	0.0032	0.01307	0.00042	0.86	83.7	2.6
X10/47	7	209	497	0.42	0.0877	0.0038	0.01300	0.00042	0.76	83.3	2.6
X10/48	10	245	746	0.33	0.0874	0.0034	0.01305	0.00042	0.82	83.6	2.6
X10/49	6	255	441	0.58	0.0908	0.0042	0.01296	0.00042	0.70	83.0	2.6
X10/50	3	105	237	0.45	0.0857	0.0042	0.01302	0.00042	0.66	83.4	2.6

S16X19					**2 σ error**		**2 σ error**	**Rho**	**Age (Ma)**	**2 σ error**

Gourbet, L., Yang, R., Fellin, M.G., Paquette, J.-L., Willett, S.D., Gong, J.F., and Maden, C., 2019, Evolution of the Yangtze River network, southeastern Tibet: Insights from thermochronology and sedimentology: Lithosphere, https://doi.org/10.1130/L1104.1
GSA Data Repository Item 2019409

zircon	Pb ppm[1]	Th ppm[1]	U ppm[1]	Th/U	$^{207}Pb/^{235}U$[2]	$^{207}Pb/^{235}U$	$^{206}Pb/^{238}U$[2]	$^{206}Pb/^{238}U$		$^{206}Pb/^{238}U$	$^{206}Pb/^{238}U$
X19/01	14	211	388	0.54	0.280	0.012	0.03330	0.00102	0.74	211.2	6.4
X19/02	19	346	514	0.67	0.232	0.009	0.03268	0.00099	0.80	207.3	6.2
X19/03	27	520	734	0.71	0.247	0.009	0.03263	0.00099	0.85	207.0	6.1
X19/04	20	368	443	0.83	0.422	0.021	0.03521	0.00111	0.63	223.1	7.0
X19/05	18	252	521	0.48	0.245	0.009	0.03258	0.00096	0.79	206.7	6.0
X19/06	31	511	751	0.68	0.454	0.017	0.03291	0.00108	0.90	208.7	6.8
X19/07	33	77	206	0.38	1.514	0.055	0.15192	0.00498	0.91	912	28
X19/08	42	148	285	0.52	1.328	0.047	0.13935	0.00456	0.92	841	26
X19/09	24	338	597	0.57	0.494	0.018	0.03289	0.00108	0.88	208.6	6.8
X19/10	34	710	672	1.06	0.697	0.024	0.03382	0.00108	0.91	214.4	6.8
X19/11	16	245	383	0.64	0.513	0.020	0.03373	0.00108	0.84	213.8	6.8
X19/12	20	310	511	0.61	0.412	0.016	0.03283	0.00105	0.85	208.3	6.6
X19/13	115	162	1032	0.16	1.072	0.037	0.11489	0.00363	0.92	701	21
X19/14	12	188	253	0.74	0.669	0.025	0.03476	0.00111	0.84	220.3	7.0
X19/15	18	332	478	0.70	0.302	0.011	0.03274	0.00102	0.82	207.6	6.5
X19/16	151	232	1152	0.20	1.337	0.047	0.13381	0.00420	0.89	810	24
X19/17	27	557	711	0.78	0.253	0.009	0.03282	0.00102	0.85	208.1	6.3
X19/18	32	530	688	0.77	0.631	0.022	0.03374	0.00105	0.88	213.9	6.5
X19/19	24	541	645	0.84	0.238	0.009	0.03258	0.00099	0.84	206.7	6.2
X19/20	13	221	285	0.78	0.301	0.013	0.04140	0.00129	0.73	261.5	7.9
X19/21	38	570	801	0.71	0.695	0.023	0.03508	0.00108	0.94	222.3	6.6
X19/22	53	270	328	0.82	1.428	0.049	0.13912	0.00423	0.89	840	24
X19/23	26	438	586	0.75	0.497	0.017	0.03419	0.00102	0.86	216.7	6.4
X19/24	32	749	775	0.97	0.404	0.014	0.03355	0.00102	0.88	212.7	6.3
X19/25	21	383	553	0.69	0.310	0.011	0.03309	0.00099	0.83	209.9	6.2
X19/26	11	177	259	0.68	0.541	0.024	0.03363	0.00105	0.72	213.2	6.5
X19/27	12	333	292	1.14	0.494	0.020	0.03342	0.00102	0.75	211.9	6.3

[1]: concentration uncertainty c.20%

[2]: data not corrected for common-Pb

Gourbet, L., Yang, R., Fellin, M.G., Paquette, J.-L., Willett, S.D., Gong, J.F., and Maden, C., 2019, Evolution of the Yangtze River network, southeastern Tibet: Insights from thermochronology and sedimentology: Lithosphere, https://doi.org/10.1130/L1104.1
GSA Data Repository Item 2019409

3. Zircon U-Th zonation

Supplementary table ST3: Zircon U-Th data obtained by in situ Laser Ablation ICP-MS

S16X10		***Centre***				***Rim***		
zircon	**Pb ppm[1]**	**Th ppm[1]**	**U ppm[1]**	**Th/U**	**Pb ppm[1]**	**Th ppm[1]**	**U ppm[1]**	**Th/U**
X10/01	3.6	123	262	0.47	19	258	1412	0.18
X10/02	14	678	916	0.74	28	1674	1750	0.96
X10/03	4.5	155	338	0.46	22	313	1688	0.19
X10/04	4.4	103	337	0.31	50	2171	3547	0.61
X10/05	39	959	2925	0.33	21	1057	1514	0.70
X10/06	13	354	977	0.36	14	274	1149	0.24
X10/07	5.7	184	419	0.44	4.2	138	343	0.40
X10/08	27	1601	1751	0.91	18	323	1429	0.23
X10/09	18	566	1292	0.44	14	248	1102	0.22
X10/10	21	623	1532	0.41	37	892	2730	0.33
X10/11	18	560	1376	0.41	25	521	1799	0.29
X10/12	7.6	315	560	0.56	17	217	1271	0.17
X10/13	9.6	338	712	0.47	80	906	6966	0.13
X10/14	9.3	234	721	0.33	22	303	1621	0.19
X10/15	6.2	298	440	0.68	70	841	6402	0.13
X10/16	4.8	163	363	0.45	23	422	1346	0.31
X10/17	9.1	419	646	0.65	16	271	1218	0.22
X10/18	7.1	219	533	0.41	6.5	167	512	0.33
X10/19	14	391	1050	0.37	18	463	1332	0.35
X10/20	19	513	1434	0.36	26	438	1988	0.22
X10/21	7.9	262	601	0.44	14	420	1028	0.41
X10/22	9.7	526	665	0.79	4.4	110	335	0.33
X10/23	6.2	224	460	0.49	30	338	2257	0.15
X10/24	2.3	87	167	0.52	6.6	303	526	0.58
X10/25	9.3	306	695	0.44	12	259	894	0.29
X10/26	6.6	432	443	0.98	16	307	1326	0.23
X10/27	9.0	315	659	0.48	16	349	1219	0.29
X10/28	19	551	1417	0.39	24	466	1704	0.27
X10/29	9.5	405	692	0.59	23	386	1803	0.21
X10/30	10	431	745	0.58	7.4	299	528	0.57
X10/31	8.3	210	641	0.33	15	276	1137	0.24
X10/32	13	573	924	0.62	17	328	1241	0.26
Mean	**11.4**	**410**	**834**	**0.51**	**22.4**	**492**	**1722**	**0.32**
STDEV	**7.5**	**291**	**554**	**0.17**	**16.8**	**442**	**1460**	**0.18**

[1]: concentration uncertainty c.20%

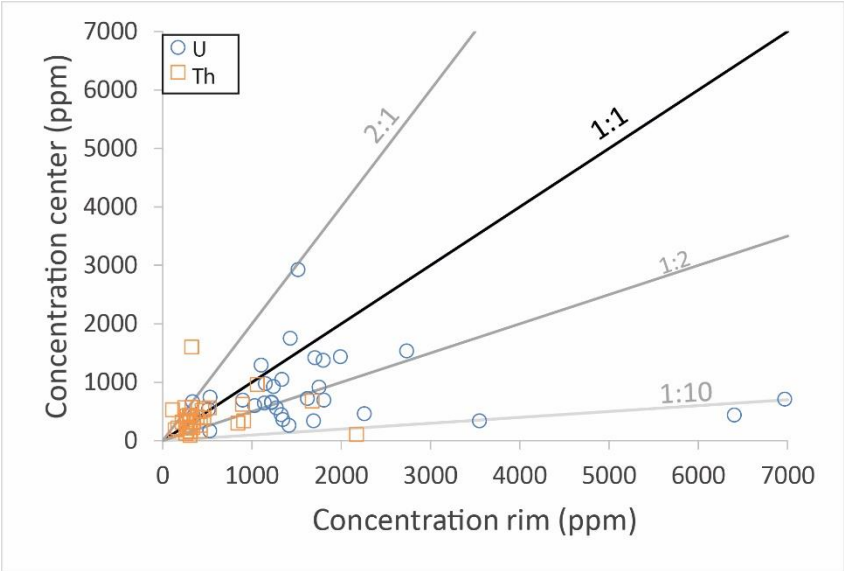

Figure S2. Zircon zonation plot showing the U and Th concentration for 32 zircon grains of sample S16X10, in the crystals centers and rims.

4. (U-Th)/He thermochronometry

4.1. Error calculation

The sample age error was calculated using the analytical uncertainties in U, Th, He measurements (and Sm for apatite) and the variance of the individual grain ages. To assess the reproducibility and accuracy of the analyses, we also measured 12 Durango apatite shards and 7 Fish Canyon Tuff zircon grains. The difference between the apatite shards ages and the nominal Durango apatite age (31.44 +/- 0.18 Ma based on K-Ar dating, McDowell et al., 2005) is 2% and the dispersion of the individual Durango apatite shards is 0.4 %. For the Fish Canyon Tuff zircon grains, the dispersion is 6.7% and the ages are in good agreement with the nominal ZHe age of 28.3 Ma from Reiners (2005) with a difference of 2.4%.

Gourbet, L., Yang, R., Fellin, M.G., Paquette, J.-L., Willett, S.D., Gong, J.F., and Maden, C., 2019, Evolution of the Yangtze River network, southeastern Tibet: Insights from thermochronology and sedimentology: Lithosphere, https://doi.org/10.1130/L1104.1
GSA Data Repository Item 2019409

4.2. Data dispersion

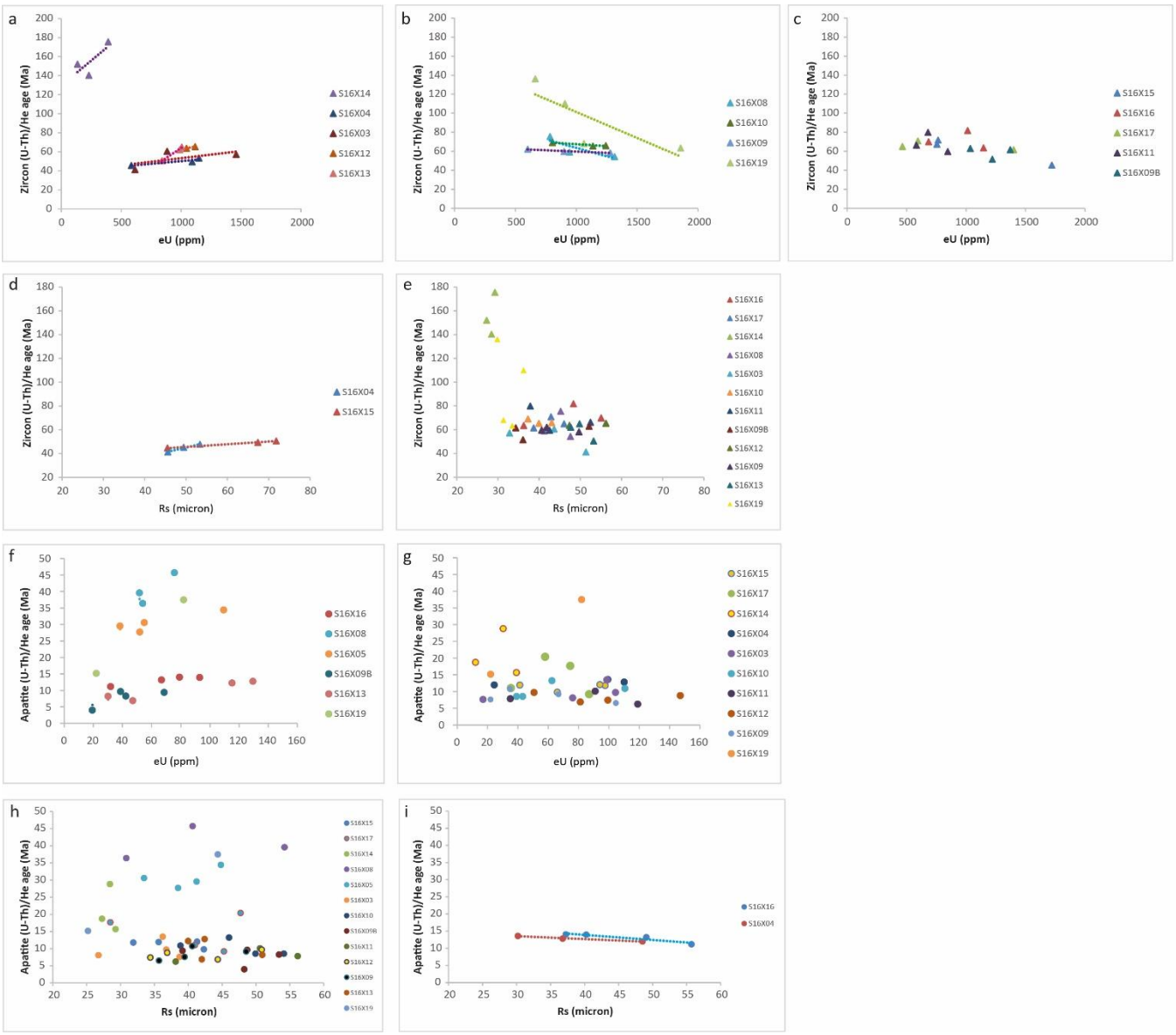

Figure S3. a.-c. Plot of eU versus ZHe age. Each data point corresponds to a single grain age. a. ZHe samples with a positive correlation between eU and age. b. ZHe samples with a negative correlation between eU and age. c. ZHe samples with no clear correlation between eU and ages. d.-e. Plot of equivalent sphere radius Rs versus ZHe age. f. Plot of eU versus single AHe ages of samples with a positive correlation between eU and age. g. Plot of eU versus single AHe ages of samples with a poor or no correlation between eU and age. h. Plot of Rs versus AHe ages for samples with a negative correlation between age and grain dimension. i. Plot of Rs versus AHe ages with a poor or no correlation between age and grain dimension.

Gourbet, L., Yang, R., Fellin, M.G., Paquette, J.-L., Willett, S.D., Gong, J.F., and Maden, C., 2019, Evolution of the Yangtze River network, southeastern Tibet: Insights from thermochronology and sedimentology: Lithosphere, https://doi.org/10.1130/L1104.1
GSA Data Repository Item 2019409

5. QTQt inverse modelling of thermochronometric data

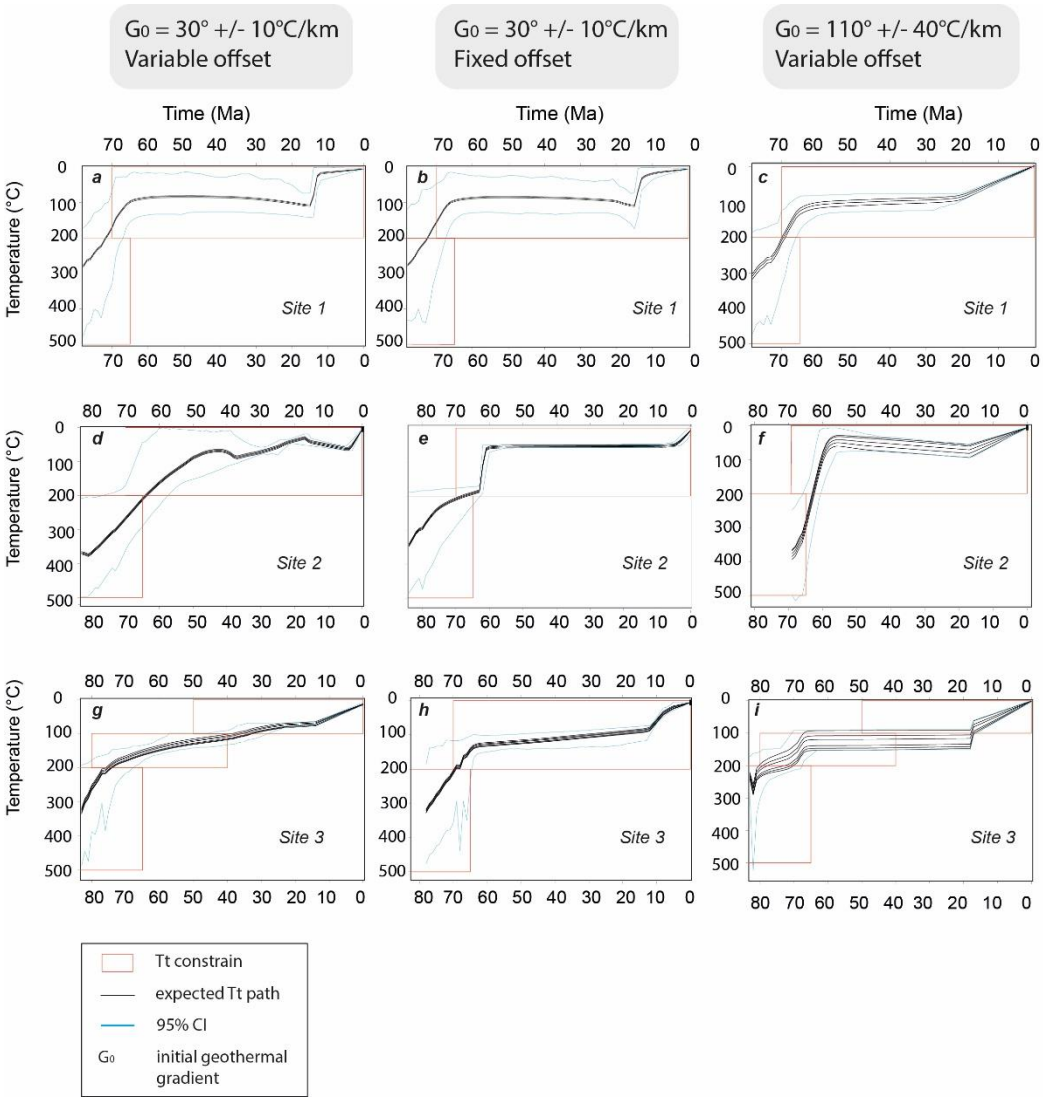

Figure S4. Additionnal thermal models of thermochronometric samples of the Cilicuo intrusion. Each black line corresponds to one sample. a, d, g: the initial geothermal gradient is set at 30+/-10°C/km, and is free to vary between 20 and 40 °C/km during the simulation (i.e. the temperature offset bewteen the highest elevation and lowest elevation samples is allowed to vary). b, e, h: the initial geothermal gradient is set at 30+/-10°C/km and remains fixed during the simulation except for the final cooling phase. c, f, i: the initial geothermal gradient is set at 110+/-40°C/km and is free to vary during the simulation.